Understanding the Role of Nanoparticle Synthesis on Their Underlying Electrocatalytic Activity

Han-Pu Liang,*,† Timothy G. J. Jones,† Nathan S. Lawrence,*,† Li Jiang,‡ and Jonathan S. Barnard§

Schlumberger Cambridge Research, High Cross, Madingley Road, Cambridge, CB3 0EL, United Kingdom, Schlumberger-Doll Research, 1 Hampshire Street, Cambridge, Massachusetts 02139, and Department of Materials Science and Metallurgy, University of Cambridge, Pembroke Street, Cambridge CB2 3QZ, United Kingdom

Received: October 17, 2007; In Final Form: January 3, 2008

Au/Pt bimetallic nanoparticles with controllable structure were fabricated and extensively characterized by transmission electron microscopy, scanning electron microscopy, energy dispersive X-ray analysis, high-resolution TEM, powder X-ray diffraction, UV−visible absorption spectroscopy and cyclic voltammetry. Their catalytic activity has been studied and compared with different Pt nanoparticles in both the electrochemical reduction of oxygen and the oxidation of methanol to investigate the role of nanoparticle synthesis on their underlying electrocatalytic activity. Enhanced signals for methanol oxidation were observed at the Au/Pt bimetallic nanoparticles.

The use of nanostructures in catalytic processes has recently come to the forefront of catalysis research. The rapidly evolving area of nanoparticle synthesis, which allows the production of novel nanoarchitectural design, is contributing to the development of new catalysts with ever-improving activity.[1] In particular, electrocatalytic reactions are of central importance as they play a vital role in promising technologies related to both environmental and energy-related applications, such as polymer electrolyte membrane fuel cells (PEMFC) and direct methanol fuel cells (DMFC).[2]

Pt is used widely in commercial catalysts, with particular attention being paid to its use in both oxygen-reduction and methanol-oxidation based fuel cells, due to its outstanding catalytic properties. The efficiency and catalytic activity of Pt catalysts can be substantially improved by increasing the activity per unit area and decreasing the quantity of the expensive Pt catalyst. Various innovative approaches have, therefore, been proposed for the synthesis of novel nanostructured Pt in an attempt to increase the surface area of Pt catalysts by decreasing their size. Such structures include nanocubes,[3] polyhedra,[4] mesoporous films,[5] hollow nanospheres,[6] nanowires,[7] nanotubes,[8] dendritic structures,[9] multipods,[10] and nanoporous electrode.[11] A problem, however, arises; the small size of the nanoparticles (typically 1−100 nm) makes the structure unstable due to the unfavorable high surface energy of the particle, which causes them to coagulate. Therefore, capping agents, such as thiol, amines, phosphines, micelles, dendrimers, polymers, and biomolecules,[12] are normally used in the fabrication methodology to stabilize and disperse the nanoparticles. Obviously, the smaller the diameter of the particle, the stronger the interaction of the stabilizing agent's with the particle is required to be.

Although the successful synthesis of smaller nanoparticles when using suitable capping agents has been reported, care has to be applied when evaluating the catalytic activity of these nanostructures. Several questions need to be answered before the nanoparticles can be successfully deployed: (1) Will these capping agents affect the catalytic performance? (2) Is the increased surface area, by decreasing the size, catalytically effective? (3) Are there any alternative methods to increase the catalytic effective surface area, thus the catalytic properties? Herein, we fabricate several types of Pt nanoparticles and investigate their underlying electrocatalytic activity for both oxygen-reduction and methanol-oxidation. The voltammetric waves obtained are compared and the results critically appraised.

Experimental Section

All chemicals were of analytical grade supplied by Aldrich and were used as received without further purification. These were as follows: platinum (IV) chloride (99.9%), gold (III) chloride trihydrate, sodium citrate tribasic dihydrate, poly (*N*-vinyl-2-pyrrolidone) (PVP, $M_w = 55\,000$), sulfuric acid, ethylene glycol, sodium hydroxide, ascorbic acid, methanol, and hydrochloric acid. All solutions were prepared with deionized water with resistivity of at least 18.2 MΩ cm (Millipore water system).

Pt nanoparticles using PVP as a stabilizing agent were prepared in accordance with a method by Teranishi et al.[13] Briefly, a mixture of 5 mL of 6.0 mM H_2PtCl_6 aqueous solution (30 μmol of Pt), 24.5 mL of water, and 20 mL of methanol containing 30 μmol of PVP was refluxed in a 100-mL flask for 3 h under air to synthesize the PVP-protected Pt nanoparticles. A typical TEM image of Pt nanoparticles with an average diameter of 4 nm can be found in the Supporting Information (Figure S1).

"Unprotected" Pt nanoparticles were prepared according to the method by Wang et al.[14] In brief, a 100-mL ethylene glycol solution containing platinum (IV) chloride (1.93 mmol) and sodium hydroxide (0.25 M) was heated at 160 °C for 0.5 h,

* To whom correspondence should be addressed. Fax: +44 1223467004. E-mail: hliang@cambridge.oilfield.slb.com; nlawrenc@cambridge.oilfield.slb.com.

† Schlumberger Cambridge Research.

‡ Schlumberger-Doll Research.

§ Department of Materials Science and Metallurgy, University of Cambridge.

10.1021/jp7100804 CCC: $40.75
Published on Web 02/28/2008

with high-purity N_2 passing through the reaction system. The solution changes from transparent yellow to a stable black Pt colloidal solution upon completion of the reaction. A typical TEM image of unprotected Pt nanoparticles is shown in the Figure S2 of the Supporting Information.

Au/Pt core−shell and bimetallic structures have previously been prepared and characterized;[15] in the following, a modified procedure was used to fabricate Au/Pt bimetallic nanoparticles based on our previous synthesis for Au/Pd core−shell nanoparticles.[16] Briefly, small Au nanoparticle seeds were first prepared by refluxing 100 mL of aqueous solution containing 0.01 g $HAuCl_4 \cdot 3H_2O$ and 0.03 g sodium citrate in a 250-mL flask for 50 min under air. Then, two aqueous solutions (1.5 mL and 6 mL) of H_2PtCl_6 (1.0 mM) containing 0.03 g sodium citrate were added to two Au seed colloidal stock solutions (8 mL), respectively. Next, an excess amount of ascorbic acid (1 mL, 0.1 M) was added at ambient temperature to the above solutions under stirring. The obtained solution mixtures will change from red to a dark brown color in the course of 3 h, thus indicating the successful formation of Pt nanocrystals.

The catalysts' loadings were obtained as follows. In the case of Au/Pt bimetallic nanoparticles, first, it was assumed that all of the $PtCl_6^{2-}$ was reduced to Pt. A suspension containing Au/Pt bimetallic particles was obtained by concentrating 2 mL of the original suspension to 0.2 mL using a centrifuge (12 000 RPM), after which a 5-μL ($Au_{25}Pt_{75}$) or 14.3-μL ($Au_{57}Pt_{43}$) aliquot of the sample was placed on the electrode surface and put into the oven at 50 °C to allow solvent evaporation. In the case of Pt nanoparticles capped by PVP, a 33.3-μL aliquot of the original suspension was allowed to dry stepwise on the electrode surface. In the case of unprotected Pt nanoparticles, the original colloidal solution was diluted 5-fold by mixing 40 μL of the above suspension with 160 μL deionized water. Sonication was used to aid dispersion. Finally, a 5.18-μL aliquot of this new suspension was placed on the electrode surface and was allowed to dry at room temperature overnight.

For TEM probing, the obtained suspensions were dropped on a carbon-coated copper grid resting on absorbent filter paper, which rapidly wicked away the solvent and allowed the nanoparticles to be dispersed on the grid. TEM measurement was performed with a Philips TECNAI 20 transmission electron microscope. Energy dispersive X-ray analysis (EDX) was performed with an FEI XL30 ESEM FEG scanning electron microscope equipped with energy dispersive X-ray analyzer (Phoenix). High-resolution TEM images were recorded on a JEOL 4000EX-II TEM operating at 400 kV. Powder X-ray diffractions (XRD) were carried out on a Bruker Advance D8 X-ray Powder Diffractometer using Cu Kα radiation (40kV, 40mA). The UV−visible absorption data were recorded on a UV−vis spectrophotometer (UV-3101 PC, SHIMADZU).

Electrochemical measurements were recorded using a μAutoLab potentiostat (Ecochemie, Netherlands) with a standard three-electrode configuration. Pt wire (1 mm diameter, Goodfellow Metals, Cambridge, UK) provided the counter electrode, and a saturated calomel electrode (SCE, Radiometer, Copenhagen) acted as the reference. The working electrode was composed of either a glass carbon electrode (3 mm diameter) onto which the Pt particles were immobilized via solvent evaporation or a planar Pt macroelectrode (1.6 mm diameter), both purchased from Bioanalytical Systems Ltd (Kenilworth, UK). All potentials were measured with respect to the SCE.

Results and Discussion

Three types of Pt nanostructures were investigated with the response of the planar Pt macroelectrode used as a reference. The first was Pt nanoparticles fabricated using poly (*N*-vinyl-2-pyrrolidone) (PVP), the most widely used capping agent in the synthesis of nanoparticles.[13] The second set of nanoparticles was fabricated so as to obviate the need for the stabilizing agent. In this case, the nanoparticles were synthesized in an alkaline ethylene glycol solution without the addition of the capping agents. It has been proposed that these unprotected Pt nanoparticles are solely stabilized by the dielectric properties of the ethylene glycol solvent.[14] The third set was based on the formation of various bimetallic structures in which the surface concentration of Pt upon the underlying metal nanoparticle can be closely controlled. Such a technique was recently shown to aid in understanding the electrochemical response of hydrogen on Pd with the signal being critically dependent on the surface coverage of Pd on the inert Au core.[16] In the present study, Au/Pt bimetallic nanoparticles are achieved in a similar manner by homogeneously depositing Pt nanoparticles onto Au nanoparticles.

Figure 1 shows the typical TEM images of Au/Pt bimetallic nanoparticles. Accordingly, the molar ratio of these particles, $Au_{25}Pt_{75}$ and $Au_{57}Pt_{43}$, are used to label these particles. It is evident, in the case of $Au_{25}Pt_{75}$ (Figure 1a), that Pt is deposited on the Au nanoparticles in the form of nanoparticles with an average diameter of 4 nm. However, when the TEM images detailed in Figure 1B for $Au_{57}Pt_{43}$ are compared with that of the Au nanoparticles, Figure S3 of the Supporting Information, remarkably similar images are observed, making discrimination between the two different nanoparticles difficult. Therefore, confirmation of Pt presence is given by the energy dispersed X-ray (EDX) analysis of both $Au_{25}Pt_{75}$ and $Au_{57}Pt_{43}$ bimetallic nanoparticles, Figure 1, parts c and d, respectively. These prove the coexistence of Au and Pt. It is interesting to note that the relative peak ratios of Pt Lα and Au Lα vary for the different sample.

The HRTEM images of Sample $Au_{25}Pt_{75}$ and $Au_{57}Pt_{43}$ are shown in Figure 2, parts a and b, respectively. It is evident, from the HRTEM image of $Au_{25}Pt_{75}$ (Figure 2a), that the irregular raised nanoparticles on the Au surface can be identified as Pt by the careful measurement of the lattice spacing and the EDX in Figure 1c. In contrast to the data shown in Figure 2a, lowering of the Pt concentration in the feed solution results in the free assembly of Pt particles standing on a uniform Au lattice part. This is indicated by the white ellipses shown in Figure 2b for $Au_{57}Pt_{43}$. In this case, more of Au crystalline surface is exposed in comparison with that of $Au_{25}Pt_{75}$. It should be further mentioned that free Pt nanoparticles are observed in both samples.

Figure 3 details the UV−visible absorption spectra of aqueous suspensions of pure Au, and of $Au_{57}Pt_{43}$ and $Au_{25}Pt_{75}$ bimetallic nanoparticles. It can be seen that pure Au nanoparticles exhibit an absorbance peak at ca. 520 nm due to their surface plasmon resonance property originating from the collective oscillation of their conduction electrons in response to optical excitation. As increasing Pt is deposited on the Au nanoparticle, as is the case for $Au_{57}Pt_{43}$ and $Au_{25}Pt_{75}$, the absorbance peak for Au nanoparticles decays. These spectra clearly demonstrate that the Pt coverage on the surface of Au nanoparticles can be controlled by increasing the H_2PtCl_6 concentration in the synthesis feed solutions.

Figure 4 gives the XRD patterns of pure Au and of $Au_{57}Pt_{43}$ and $Au_{25}Pt_{75}$ bimetallic nanoparticles. All diffraction peaks of

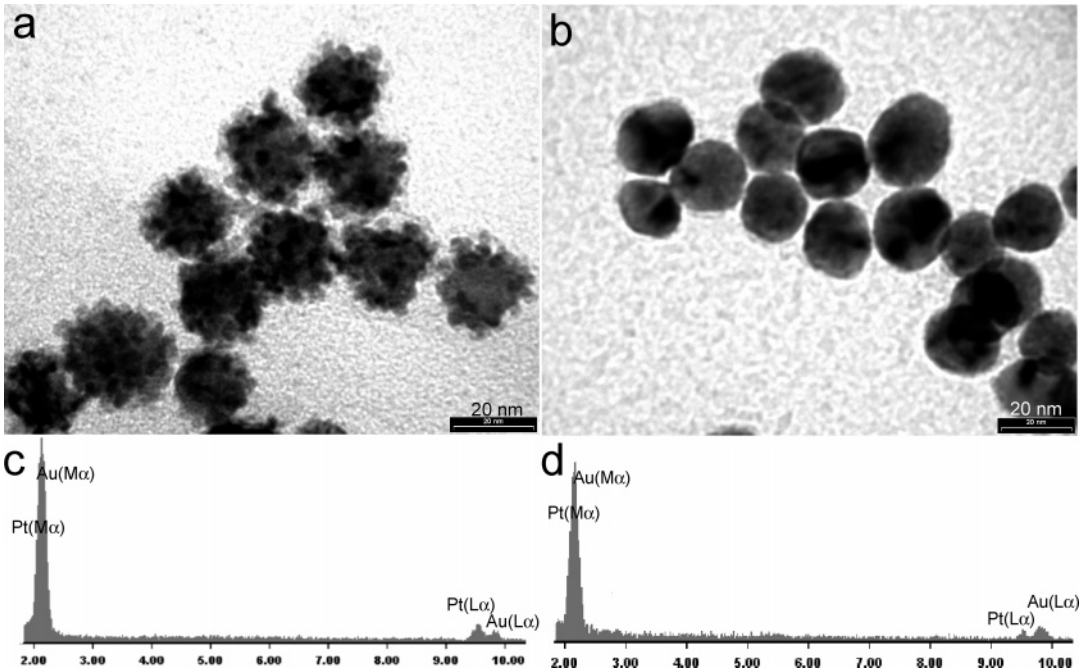

Figure 1. Typical TEM images and the energy dispersed X-ray (EDX) analysis of (a, c) $Au_{25}Pt_{75}$ and (b, d) $Au_{57}Pt_{43}$ bimetallic nanoparticles formed by reducing $PtCl_6^{2-}$ on Au nanoparticles.

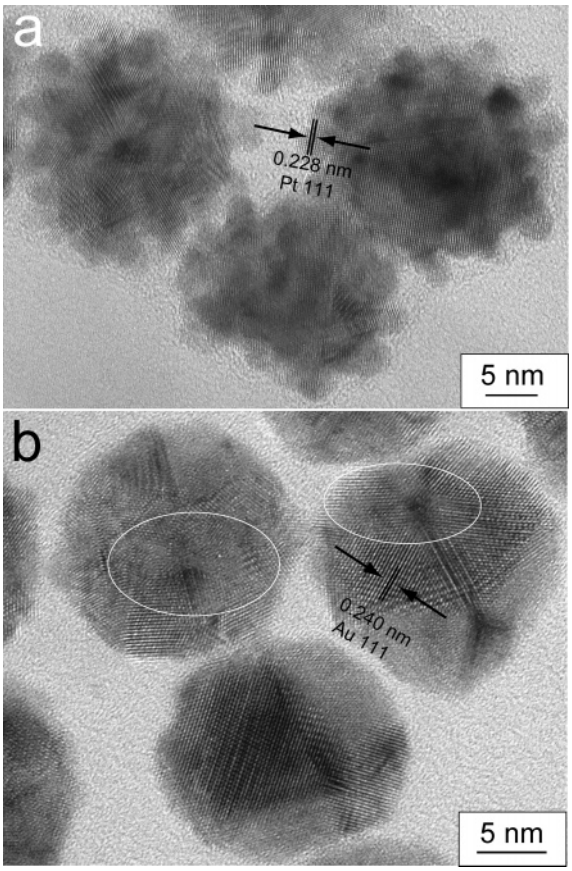

Figure 2. High-resolution TEM (HRTEM) images of (a) $Au_{25}Pt_{75}$ and (b) $Au_{57}Pt_{43}$ bimetallic nanoparticles.

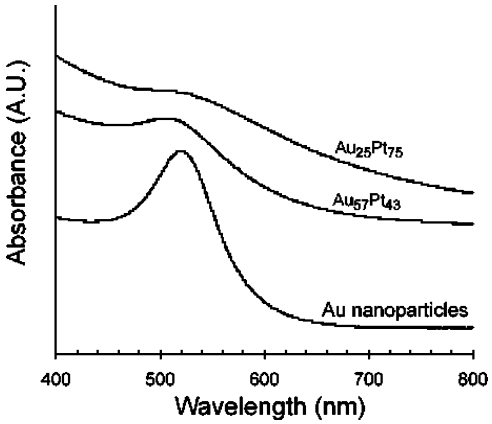

Figure 3. UV−visible absorption spectra of aqueous suspension of pure Au, and of $Au_{57}Pt_{43}$ and $Au_{25}Pt_{75}$ bimetallic nanoparticles.

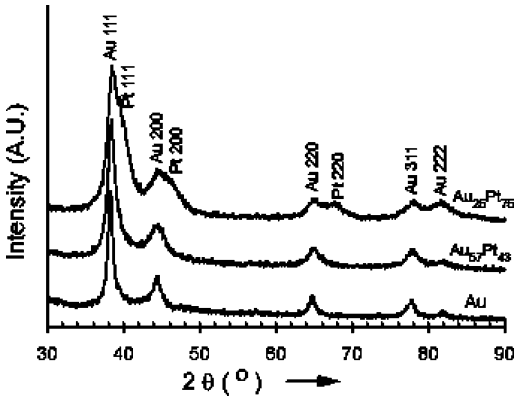

Figure 4. Typical powder X-ray diffraction (XRD) patterns of the pure Au nanoparticles, and of the bimetallic nanoparticles, $Au_{25}Pt_{75}$ and $Au_{57}Pt_{43}$, formed by reducing $PtCl_6^{2-}$ onto Au nanoparticles.

Au nanoparticles could be unambiguously indexed to the diffraction of (111), (200), (220), (311), and (222) planes of face-center-cubic (fcc) gold according to XRD standard JCPDS No. 65−2870. The diffraction peaks of pure Au and $Au_{57}Pt_{43}$ nanoparticles are difficult to distinguish, although the $Au_{57}Pt_{43}$ has broad peaks than pure Au. In the case of $Au_{25}Pt_{75}$, it is interesting to note that weak shoulder peaks at ca. 40° and ca. 47°, along with a separate peak at ca. 68°, are observed, which can be assigned to the diffraction of (111), (200), and (220) planes of fcc Pt according to the JCPDS No. 87-0647.

Electrocatalysts play a crucial role in PEMFC and DMFC. Most Pt-based electrocatalysts have been evaluated for both the

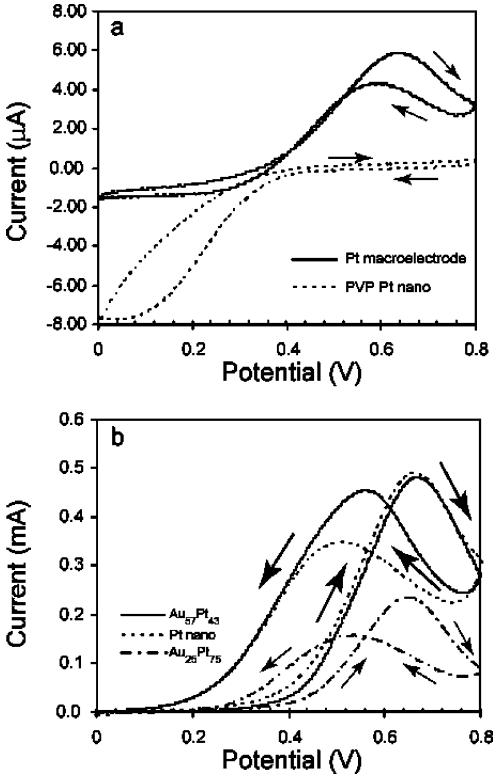

Figure 5. Cyclic voltammetric response (scan rate = 50 mV s^{-1}) of the various Pt electrode layers (a) Pt macroelectrode and PVP-coated Pt nanoparticles, and (b) the various synthesized Au/Pt bimetallic structures along with that of unprotected Pt nanoparticles, when placed in 0.5 M H_2SO_4 containing 1 M methanol. Pt loading for each sample was 20 nmol (3.9 μg). The geometric area of the planar Pt macroelectrode is 0.02 cm^2 and the geometric area of the glass carbon electrode is 0.07 cm^2.

oxygen-reduction and methanol-oxidation reactions.[3b,6b,11,17] Furthermore, considerable effort was recently directed toward using Au as nanocatalysts[18] since it has been reported that Au nanoparticles with diameter of ca. 3.5 nm supported on titania are effective for catalyzing the oxidation of carbon monoxide.[19] In addition, more recently, it has been shown that Au clusters contribute to the stabilization of Pt electrocatalysts in the oxygen-reduction reaction.[20] It is therefore of interest to investigate what role the Au nanoparticle, in the current Au/Pt bimetallic nanoparticles, may play in both the methanol-oxidation and oxygen-reduction reactions, when compared to both unprotected and PVP-capped pure Pt nanoparticles with the response of the planar Pt macroelectrode as a reference.

Figure 5 details the electrochemical signal of the various Pt electrode layers when placed in 0.5 M H_2SO_4 containing 1 M methanol. Figure 5a compares the response of the Pt macroelectrode (solid) with that of a layer containing PVP-coated Pt nanoparticles (dotted). The Pt macroelectrode produces a well-defined oxidation wave at +0.65 V. Upon a reversal of the scan direction, a hysteresis phenomenon is observed, in which an oxidative peak current at +0.56 V is recorded on the reductive sweep. In contrast, the PVP-coated Pt nanoparticle layer produces no significant response to methanol with no oxidative or hysteresis phenomenon observed. Figure 5b illustrates the response of the various synthesized Au/Pt bimetallic structures along with that of unprotected Pt nanoparticles. Note the different current scales between Figure 5, parts a and b. All three layers show well-defined oxidative waves at ca. +0.65 V with corresponding hysteresis waves at ca. +0.52 V, in agreement with results at nanoporous Pt.[11] A comparison of the

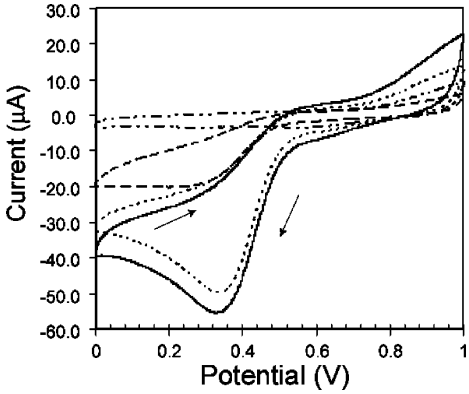

Figure 6. Electrochemical response (scan rate = 50 mV s^{-1}) of the $Au_{25}Pt_{75}$ bimetallic nanoparticles layer, containing various catalyst loadings (dashed line −10 nmol, dotted line −20 nmol, and solid line −40 nmol), when placed in an oxygen-saturated 0.5 M H_2SO_4 solution. The dot-dashed line is the electrochemical response of $Au_{25}Pt_{75}$ with 20 nmol loading in the absence of oxygen (bubbled with N_2). The geometric area of the glass carbon electrode is 0.07 cm^2.

peak currents obtained on the initial oxidative sweep shows that the $Au_{57}Pt_{43}$ and unprotected Pt nanoparticle layers produce similar currents but higher than those of the $Au_{25}Pt_{75}$ layer. In contrast, the oxidative current, observed on the reduction sweep, reveals that the $Au_{57}Pt_{43}$ electrode is greater than that of the Pt unprotected nanoparticle layer, which is larger than that of the $Au_{25}Pt_{75}$ layer.

The results detailed above compare the ability of various Pt nanoparticle layers to act as catalysts in the electrochemical oxidation of methanol. However, it was found that the PVP-coated nanoparticles, although being small in diameter (4 nm), produced the poorest response. The poor signal observed at the PVP nanoparticle layer can be attributed to the presence of the strong capping agent on the Pt nanoparticle surface, thus producing a detrimental impact on the particle's catalytic properties.[4b] The strong affinity of the PVP with the Pt nanoparticles hinders the diffusion of methanol to the Pt surface and, therefore, inhibits electron transfer from the Pt. In contrast the responses obtained at the various Au/Pt bimetallic and unprotected Pt nanoparticles are significantly improved compared to that of the Pt macroelectrode. This enhanced response can be attributed to their large effective surface area, increased mass transport, and high catalytic activity at the electrode surface. A more detailed insight into these differing voltammetric signals was provided by studying the electrochemical response of each layer for the diffusion-controlled oxygen-reduction process.

Figure 6 details the effect of catalyst loading on the electrochemical response of the Au/Pt bimetallic layer toward oxygen reduction. This clearly shows that increasing the concentration of the particles on the electrode surface from 10 to 20 nmol almost doubles the voltammetric response. However, when the loading was increased further to 40 nmol, little change in the response was observed. This limiting response can be tentatively attributed to the fact that the reduction of oxygen is a diffusion-limited process, and increasing the concentration of particles on the electrode surface further has little impact on the electroactive surface area.[17b] It should be noted that in the absence of oxygen (dot-dashed line, 20 nmol Pt loading), no voltammetric signal was recorded in the potential range studied. This further demonstrates that the well-defined reduction wave at ca. +0.32 V corresponds to the reduction of oxygen, which is in agreement with the results obtained at dendrimer-encapsulated-Pt-nanoparticles-modified glass carbon electrode[17a]

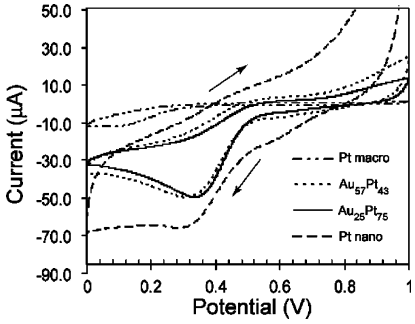

Figure 7. Cyclic voltammetric (scan rate = 50 mV s^{-1}) response of various Pt layers when placed in oxygen-saturated 0.5 M H_2SO_4 solution. Pt loading for each sample was 20 nmol (3.9 μg). The geometric area of the planar Pt macroelectrode is 0.02 cm^2 and the geometric area of the glass carbon electrodeis 0.07 cm^2.

and occurs at potentials much higher than those on an ultrathin Pt-coated-gold-nanoparticles-monolayer film electrode developed by an underpotential-deposition method.[21]

Figure 7 details the cyclic voltammetric response of four different Pt electrode layers ($Au_{57}Pt_{43}$, $Au_{25}Pt_{75}$, unprotected Pt and a planar Pt macroelectrode). In the light of the fact that the PVP-coated nanoparticles produced no defined voltammetric response for methanol oxidation, these particles were not investigated in the oxygen-reduction reaction. All of the nanoparticle layers have the same Pt loading of 20 nmol (3.9 μg). It is evident from these cyclic voltammograms that, under identical conditions, all of the Pt nanoparticle layers exhibit a significantly higher response than that of the solid planar macroelectrode. Both the Au/Pt bimetallic and the unprotected Pt nanoparticles produce well-defined reduction waves at ca. +0.32 V corresponding to the reduction of oxygen directly at the electrode surface. In contrast, only a small reduction wave at ca. +0.12 V is observed at the Pt macroelectrode. The Au/Pt bimetallic and the unprotected Pt nanoparticles produce similar catalytic responses to oxygen reduction, with the unprotected Pt nanoparticles exhibiting a slightly higher activity.

Comparison of the response of the bimetallic structures with the unprotected nanoparticles for both electrochemical systems investigated shows that, in the case of oxygen reduction, remarkably similar behavior is observed. However, contrasting behavior is recorded in the case of methanol oxidation with the $Au_{57}Pt_{43}$ bimetallic layer producing an enhanced current response on the reverse sweep. These apparently anomalous results can be rationalized as follows. In the case of oxygen reduction, the process is purely diffusion-controlled. The peak current will be dependent on the size and structure of the electroactive surface area of the nanoparticle. The $Au_{25}Pt_{75}$, $Au_{57}Pt_{43}$, and unprotected Pt nanoparticles may therefore have similar effective catalytic surface areas of Pt. The unprotected Pt exhibit the highest catalytic activity in oxygen reduction. However, this is not the case for the electrochemical oxidation of methanol although it has been shown that unprotected nanocatalysts fabricated in an analogous manner display enhanced activity when compared to commercial nanocatalysts.[22]

The difference in catalytic activity among these three nanocatalysts is greatly magnified for methanol oxidation in comparison with oxygen reduction. The electrochemical oxidation of methanol follows two parallel pathways: a fast one leading to the formation of CO_2, and a slow pathway leading to the strongly adsorbing and poisoning CO species.[23] In situ infrared reflectance spectroscopy and nuclear magnetic resonance spectroscopy have identified CO as the poisoning intermediate.[24] It can be envisaged that for both the Au/Pt bimetallic nanoparticles and the unprotected Pt nanoparticles, the two oxidation pathways will exist where CO will be formed and adsorb onto the Pt particle. The enhanced hysteresis current of the $Au_{57}Pt_{43}$ particle relative to the Pt nanoparticles and the increase in both the oxidative and hysteresis peak currents of $Au_{57}Pt_{43}$ relative to $Au_{25}Pt_{75}$ can be rationalized as follows. In order to maintain a constant Pt loading, more Au nanoparticles are used in the case of the $Au_{57}Pt_{43}$ nanoparticles because there is, on average, less Pt on the Au surface in with the $Au_{25}Pt_{75}$, as can be seen from the TEM images in Figure 1. This is further confirmed from the SEM images of $Au_{25}Pt_{75}$ and$Au_{57}Pt_{43}$, Figures S4 and S5 of the Supporting Information respectively, which show the arrangement of nanoparticles on the electrode surface. The $Au_{25}Pt_{75}$ form island structures on the electrode surface while $Au_{57}Pt_{43}$ forms a film structure, the different morphologies can be attributed to the variation in Au nanoparticle loading between the two samples. In addition, there is relatively more exposed Au surface on nearly every $Au_{57}Pt_{43}$ nanoparticles (Figure 2). This exposed Au is in contact with the Pt particle and can effectively oxidize the adsorbed CO species to CO_2, as Au nanoparticles are well-known to be highly active, low-temperature CO-oxidation catalysts,[15a, 25] although adsorption of CO is supposed to occur on the Pt species. The oxidation of CO on the adjacent Au surface effectively regenerates the Pt surface to allow further methanol oxidation to occur. A more detailed mechanism of the gold surfaces ability to oxidize CO is given elsewhere. In this case, it was shown that Au could catalyze CO oxidation at low temperature.[25g] In the case of the unprotected Pt, this is not the case; no regeneration of the surface can occur, and hence, its catalytic property is diminished. Furthermore, analysis of the TEM images detailed in Figures 1 and 2 clearly show some differences of the particle surface morphologies. It can be envisaged that the surface morphology will also play an important role in the differing catalytic activity of the various nanoparticle layers. However, the results reported here highlights that $Au_{57}Pt_{43}$ nanoparticles are highly efficient electrocatalysts for methanol oxidation. This may represent a new, relatively inexpensive, promising electrocatalyst for DMFC in comparison with the expensive PtRu catalysts, which are postulated to result from both electronic and structural effects of the bimetal.[26]

Conclusions

In summary, we have demonstrated that when using nanoparticles in catalytic applications, judicious choice of the pathways to synthesize the nanoparticles needs to be applied because their final surface morphology greatly affects their underlying electrocatalytic activity. The presence of capping agents substantially affects their catalytic performance, and the increased surface area so formed is not catalytically effective under these circumstances. The long-chain capping agent (PVP) covers the Pt surface and, thereby, inhibits the catalytic activity. However, the unprotected nanoparticles stabilized by the solvent can exhibit high catalytic activity.

Deployment of bimetallic nanoparticles has demonstrated another effective strategy to improve the catalytic activity. On the one hand, smaller nanoparticles can be deposited on larger nanoparticles using weak capping agents. On the other hand, the larger nanoparticles can play a significant role in promoting electrocatalysis, as demonstrated for the electrochemical oxidation of methanol by Au/Pt nanoparticles. Our studies raise promising possibilities in developing improved DMFC electrocatalysts, while also shedding critical light in the design of architectural nanocatalysts for other catalyst-related research fields.

Acknowledgment. The authors thank Graeme Langlands for conducting the XRD experiments.

Supporting Information Available: TEM and SEM images. This information is available free of charge via the Internet at http://pubs.acs.org.

References and Notes

(1) (a) Grunes, J.; Zhu, J.; Somorjai, G. A. *Chem. Commun.* **2003**, 2257. (b) Bell, A. T. *Science* **2003**, *299*, 1688. (c) D. R. Rolison, *Science* **2003**, *299*, 1698. (d) Schlögl, R.; Hamid, S. B. A. *Angew. Chem. Int. Ed.* **2004**, *43*, 1628. (e) Wang, J.; Scampicchio, M.; Laocharoensuk, R.; Valentini, F.; Gonzalez-Garcia, O.; Burdick, J. *J. Am. Chem. Soc.* **2006**, *128*, 4562. (f) Wieckowski, A.; Savinova, E. R.; Vayenas, C. G. *Catalysis and Electrocatalysis at Nanoparticle Surface*; CRC Press: Boca Raton, 2003.

(2) (a) Raimondi, F.; Scherer, G. G.; Kötz, R.; Wokaun. A. *Angew. Chem. Int. Ed.* **2005**, *44*, 2190. (b) Liu, H. S.; Song, C. J.; Zhang, L.; Zhang, J. J.; Wang, H. J.; Wilkinson. D. P. *J. Power Sources* **2006**, *155*, 95.

(3) (a) Ahmadi, T. S.; Wang, Z. L.; Green, T. C.; Henglein, A.; Elsayed, M. A. *Science* **1996**, *272*, 1924. (b) Wang, C.; Daimon, H.; Lee, Y.; Kim, J.; Sun, S. *J. Am. Chem. Soc.* **2007**, *129*, 6974. (c) Lee, H.; Habas, S. E.; Kweskin, S.; Butcher, D.; Somorjai, G. A.; Yang. P. *Angew. Chem. Int. Ed.* **2006**, *45*, 7824.

(4) (a) Tian, N.; Zhou, Z.-Y.; Sun, S.-G.; Ding, Y.; Wang, Z. L. *Science* **2007**, *316*, 732. (b) Song, H.; Kim, F.; Connor, S.; Somorjai, G. A.; Yang, P. *J. Phys. Chem. B* **2005**, *109*, 188.

(5) Attard, G. S.; Bartlett, P. N.; Coleman, N. R. B.; Elliott, J. M.; Owen, J. R.; Wang, J. H. *Science* **1997**, *278*, 838.

(6) (a) Mayers, B.; Jiang, X.; Sunderland, D. Cattle, B.; Xia, Y. *J. Am. Chem. Soc.* **2003**, *125*, 13364. (b) Liang, H.-P.; Zhang, H.-M.; Hu, J.-S.; Guo, Y.-G.; Wan, L.-J.; Bai, C. -L. *Angew. Chem. Int. Ed.* **2004**, *43*, 1540. (c) Song, Y. J.; Garcia, R. M.; Dorin, R. M.; Wang, H. R.; Qiu, Y.; Shelnutt, J. A. *Angew. Chem. Int. Ed.* **2006**, *45*, 8126.

(7) Chen, J. Y.; Herricks, T.; Geissler, M.; Xia, Y. N. *J. Am. Chem. Soc.* **2004**, *126*, 10854.

(8) (a) Luo, Y.; Lee, S. K.; Hofmeister, H.; Steinhart, M.; Gösele, U. *Nano Lett.* **2004**, *4*, 143. (b) Mu Y.-Y.; Liang, H. -P.; Hu, J.-S.; Wan, L.-J. *J. Nanosci. Nanotechnol.* **2005**, *5*, 1929. (c) Guo, Y.-G.; Hu, J.-S.; Zhang, H.-M.; Liang, H.-P.; Wan, L.-J.; Bai, C. -L. *Adv. Mater.* **2005**, *17*, 746. (d) Kijima, T.; Yoshimura, T.; Uota, M. *Angew. Chem. Int. Ed.* **2004**, *43*, 228.

(9) (a) Song, Y.; Yang, Y.; Medforth, C. J.; Pereira, E.; Singh, A. K.; Xu, H. Jiang, Y.; Brinker, C. J.; van Swol, F.; Sheinutt, J. A. *J. Am. Chem. Soc.* **2004**, *126*, 635. (b) Teng, X. W.; Liang, X.-Y.; Maksimuk, S.; Yang, H. *Small* **2006**, *2*, 249. (c)X. Zhong, Y. Feng, I. Lieberwirth, W. Knoll, *Chem. Mater.* **2006**, *18*, 2468.

(10) a) X. Teng, H. Yang *Nano Letters* **2005**, *5*, 885; b) H. -P. Liang, J. -S. Hu, A. -M. Cao, Y. -Y. Mu, L. -J. Wan, *J. Nanosci. Nanotechnol.* **2006**, *6*, 2031.

(11) Hu, Y.-S; Guo, Y.-G.; Sigle, W.; Hore, S.; Balaya, P.; Maier, J. *Nat. Mater.* **2006**, *5*, 713.

(12) (a) Roucoux, A.; Schulz, J.; Patin, H. *Chem. Rev.* **2002**, *102*, 3757. (b) Niemeyer, C. M. *Angew. Chem. Int. Ed.* **2001**, *40*, 4129.

(13) Teranishi, T.; Hosoe, M.; Tanaka, T.; Miyake, M. *J. Phys. Chem. B* **1999**, *103*, 3818.

(14) Wang, Y.; Ren, J.; Deng, K.; Gui, L.; Tang, Y. *Chem. Mater.* **2000**, *12*, 1622.

(15) For example: (a) Zhou, S.; Mcllwrath, K.; Jackson, G.; Eichhorn, B. *J. Am. Chem. Soc.* **2006**, *128*, 1780. (b) Zhong, C.-J.; Maye, M. M. *Adv. Mater.* **2001**, *13*, 1507. (c) Liang, H.-P.; Guo, Y.-G.; Zhang, H.-M.; Hu, J.-S.; Wan, L.-J.; Bai, C. -L. *Chem. Commun.* **2004**, 1496. (d) Henglein, A. *J. Phys. Chem. B* **2000**, *104*, 2201. (e) Wu, M.-L.; Chen, D.-H.; Huang, T.-C. *Chem. Mater.* **2001**, *13*, 599. (f) Luo, J.; Maye, M. M.; Petkov, V.; Kariuki, N. N.; Wang, L.; Njoki, P.; Mott, D.; Lin, Y.; Zhong, C. J. *Chem. Mater.* **2005**, *17*, 3086. (g) Zhao, D.; Xu, B.-Q. *Angew. Chem. Int. Ed.* **2006**, *45*, 4955.

(16) Liang, H.-P.; Lawrence, N. S.; Jones, T. G. J.; Banks, C. E.; Ducati, C. *J. Am. Chem. Soc.* **2007**, *129*, 6068.

(17) For example: (a) Ye, H.; Crooks, R. M. *J. Am. Chem. Soc.* **2005**, *127*, 4930. (b) Cui, G.; Zhi, L, Thomas, A.; Kolb, U.; Lieberwirth, I.; Müllen, K. *Angew. Chem. Int. Ed.* **2007**, *46*, 3464. (c) Zhang, J.; Vukmirovic, M. B.; Sasaki, K.; Nilekar, A. U.; Mavrikakis, M.; Adzic, R. R. *J. Am. Chem. Soc.* **2005**, *127*, 12480. (d) Ye, H.; Crooks, R. M. *J. Am. Chem. Soc.* **2007**, *129*, 3627.

(18) (a) Corma, A.; Serna, P. *Science* **2006**, *313*, 332. (b) Hughes, M. D.; Xu, Y.-J.; Jenkins, P.; McMorn, P.; Landon, P.; Enache, D. I.; Carley, A. F.; Attard, G. A.; Hutchings, G. J.; King, F.; Hugh Stitt, E.; Johnston, P.; Griffin, K.; Kiely, C. J. *Nature* **2005**, *437*, 1132.

(19) Valden, M.; Lai, X.; Goodman, D. W. *Science* **1998**, *281*, 1647.

(20) Zhang, J.; Sasaki, K.; Sutter, E.; Adzic, R. R. *Science* **2007**, *315*, 220.

(21) Jin, Y.; Shen, Y.; Dong, S. *J. Phys. Chem. B* **2004**, *108*, 8142.

(22) Bock, C.; Paquet, C.; Couillard, M.; Botton, G. A.; MacDougall, B. R. *J. Am. Chem. Soc.* **2004**, *126*, 8028.

(23) (a) Parsons. R.; Van der Noot, T. *J. Electroanal. Chem.* **1988**, *257*, 9. (b) Herrero, E.; Chrzanowski, W.; Wieckowski. A. *J. Phys. Chem.* **1995**, *99*, 10423.

(24) (a) Beden, B.; Lamy, C.; Bewick, A.; Kunimatsu, K. *J. Electroanal. Chem.* **1981**, *121*, 343. (b) Day, J. B.; Vuissoz, P.-A.; Oldfield, E.; Wieckowski, A.; Ansermet, J.-P. *J. Am. Chem. Soc.* **1996**, *118*, 13046.

(25) (a) Comotti, M.; Li, W. C.; Spliethoff, B.; Schuth, F. *J. Am. Chem. Soc.* **2006**, *128*, 917. (b) Xu, C.; Su, J.; Xu, X.; Liu, P.; Zhao, H.; Tian, F.; Ding, Y. *J. Am. Chem. Soc.* **2007**, *129*, 42. (c) Kim, T. S.; Stiehl, J. D.; Reeves, C. T.; Meyer, R. J.; Mullins, C. B. *J. Am. Chem. Soc.* **2003**, *125*, 2018. (d) Fu, Q. Saltsburg, H.; Flytzani-Stephanopoulos, M. *Science* **2003**, *301*, 935. (e) Yan, W.; Mahurin, S. M.; Pan, Z.; Overbury, S. H.; Dai, S. *J. Am. Chem. Soc.* **2006**, *127*, 10480. (f) Diao, P.; Zhang, D. F.; Guo M.; Zhang, Q. *J. Catal.* **2007**, *250*, 247. (g) Kung, M. C.; Davis, R. J.; Kung, H. H. J. Phys. Chem. C 2007, 111, 11767.

(26) (a) Yajima, T.; Uchida, H.; Watanabe, M. *J. Phys. Chem. B* **2004**, *108*, 2654. (b) Tong, Y. Y.; Kim, H. S.; Babu, P. K.; Waszczuk, P.; Wieckowski, A.; Oldfield, E. *J. Am. Chem. Soc.* **2002**, *124*, 468.